Cryo-EM analysis of a domain antibody bound rotary ATPase complex

Roberta B Davies[1,2], Callum Smits[1], Andrew SW Wong[3], Daniela Stock[1,4], Mary Christie[1,4], Sara Sandin[3,5] and Alastair G Stewart[1,4]

[1]Molecular, Structural and Computational Biology Division, The Victor Chang Cardiac Research Institute, Darlinghurst, NSW 2010, Australia.
[2]Current address: School of Physics, The University of New South Wales, NSW 2052, Australia.
[3]NTU Institute of Structural Biology, Nanyang Technological University, 636921, Singapore.
[4]Faculty of Medicine, The University of New South Wales, Sydney, NSW 2052, Australia.
[5]School of Biological Sciences, Nanyang Technological University, 637551, Singapore.

Abstract
The bacterial A/V-type ATPase/synthase rotary motor couples ATP hydrolysis/synthesis with proton translocation across biological membranes. The A/V-type ATPase/synthase from *Thermus thermophilus* has been extensively studied both structurally and functionally for many years. Here we provide an 8.7 Å resolution cryo-electron microscopy 3D reconstruction of this complex bound to single-domain antibody fragments, small monomeric antibodies containing just the variable heavy domain. Docking of known structures into the density revealed the molecular orientation of the domain antibodies, suggesting that structure determination of co-domain antibody:protein complexes could be a useful avenue for unstable or smaller proteins. Although previous studies suggested that the presence of fluoroaluminate in this complex could change the rotary state of this enzyme, we observed no gross structural rearrangements under these conditions.

Rotary ATPases couple ATP turnover with ion translocation through membranes and are central to biological energy conversion (Stewart et al., 2014). Although there are many different subtypes of rotary ATPases found across all known forms of life (Stewart et al., 2014), some bacteria contain a single type of rotary ATPase termed the bacterial A/V-type ATPase/synthase (Nakano et al., 2008). These complexes are bifunctional, being able to either utilize the proton motive force to synthesize ATP, or use energy derived from ATP hydrolysis to pump ions across membranes depending on their local environment (Nakano et al., 2008).

Rotary ATPases have been amenable targets for electron cryo microscopy (cryo-EM) studies owing to their relatively large size, and hence moderate to high resolution maps have been determined utilising recent advances in electron detection techniques and processing (Allegretti et al., 2015; Hahn et al., 2016; Mazhab-Jafari et al., 2016; Schep et al., 2016; Sobti et al., 2016; Vinothkumar et al., 2016; Zhao et al., 2015). The bacterial A/V-type ATPase/synthase from the thermophilic eubacterium *Thermus thermophilus* was first subjected to negative stain electron microscopy single particle averaging over a decade ago, resulting in a 23 Å map that highlighted two peripheral stalks and the overall architecture of the complex (Bernal and Stock, 2004). As techniques and equipment improved, the resolution of these maps steadily increased (Lau and Rubinstein, 2010, 2011), resulting in a moderate resolution map to 6.4 Å resolution (Schep et al., 2016).

Prior to cryo-EM information, the stoichiometry and localization of the peripheral stalks in this complex was established using second-generation synthetic human variable heavy (V_H) domain antibody fragments (dAbs) initially derived using phage

display selections against the EG heterodimeric subunit as antigen (Esteban et al., 2008). These dAbs have since proven useful for purifying native protein from the host organism for other applications such as ion mobility-mass spectrometry (Zhou et al., 2014).

Here for the first time we show the A/V-type ATPase/synthase from *T. thermophilus* bound to dAbs using cryo-EM. The map has a resolution of 8.7 Å, as determined by the gold-standard method (Henderson et al., 2012; Scheres, 2012). The reconstruction shows the precise location of a single dAb on each of the two peripheral stalks, with what appears to be full occupancy.

T. thermophilus A/V-ATPase:dAb complex was purified as described previously (Esteban et al., 2013) with the following changes. Cells were grown at 65 °C (150 revolutions per minute) to stationary phase, and digitonin was used instead of DDM to purify the complex from membranes. After size exclusion chromatography, the purified protein was serially incubated on ice to exchange the nucleotide, as has been previously reported (Braig et al., 2000); first with 2 mM ADP and 10 mM $MgCl_2$ for 20 minutes, then 5 mM NaF for 20 minutes, and finally 1 mM $AlCl_3$ for one hour. Aliquots of 4 µl of purified *T. thermophilus* A/V-ATPase:dAb complex at a concentration of 2.9 µM were placed on glow-discharged holey carbon grids (Quantifoils Copper R2/2, 200 Mesh). Grids were blotted for 2 s and flash-frozen in liquid ethane using an FEI Vitrobot Mark IV. Grids were transferred to an FEI Talos Arctica transmission electron microscope operating at 200 kV. Images were recorded automatically using the FEI EPU software, yielding a pixel size of 1.91 Å. A dose rate of 13.3 to 14.3 electrons (spread over 7 frames) per $Å^2$ per second, and an exposure

time of 1.35 s were used on the Falcon-II detector. 881 movies were collected, and a representative micrograph can be seen in Figure 1A.

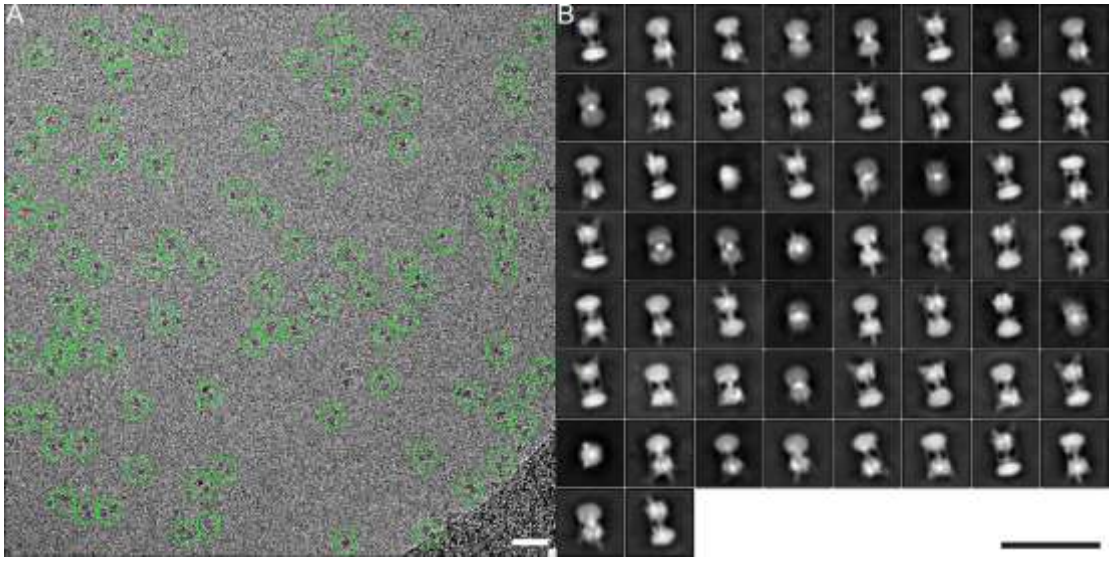

Figure 1: Electron micrograph and 2D class averages. (A) Representative micrograph with picked particles circled in green, white scale bar represents 500 Å. (B) 58 2D classes of 77,612 particles picked across the dataset, black scale bar represents 500 Å.

MotionCorr (Li et al., 2013) was used to correct local beam-induced motion and to sum the frames. Defocus and astigmatism values were estimated using CTFFIND4 (Rohou and Grigorieff, 2015). 1002 particles were manually picked and subjected to 2D classification to generate templates for autopicking in RELION (Scheres, 2012), after which a total of 147,513 particles were identified. These particles were then subjected to two rounds of 2D classification to generate 58 classes (Figure 1B) containing 77,612 particles. These particles were further classified into four 3D classes using a reconstruction from a previously published *T. thermophilus* rotary ATPase structure (Schep et al., 2016), low pass filtered to 60 Å. Three of these classes looked similar and contained the majority of the particles and were combined to

create a set containing 68,234 particles. These particles were movie refined and polished before a final 3D classification was performed. Particles from the three best classes were merged to create a final set of 61,045 particles, which were averaged to create the final map (Figure 2A). The resolution was estimated using Fourier Shell Correlation (FSC= 0.143, gold-standard – Supplementary Figure 1) giving a final resolution of 8.7 Å. Supplementary Figure 2 is a summary of these methods, shown as a flowchart.

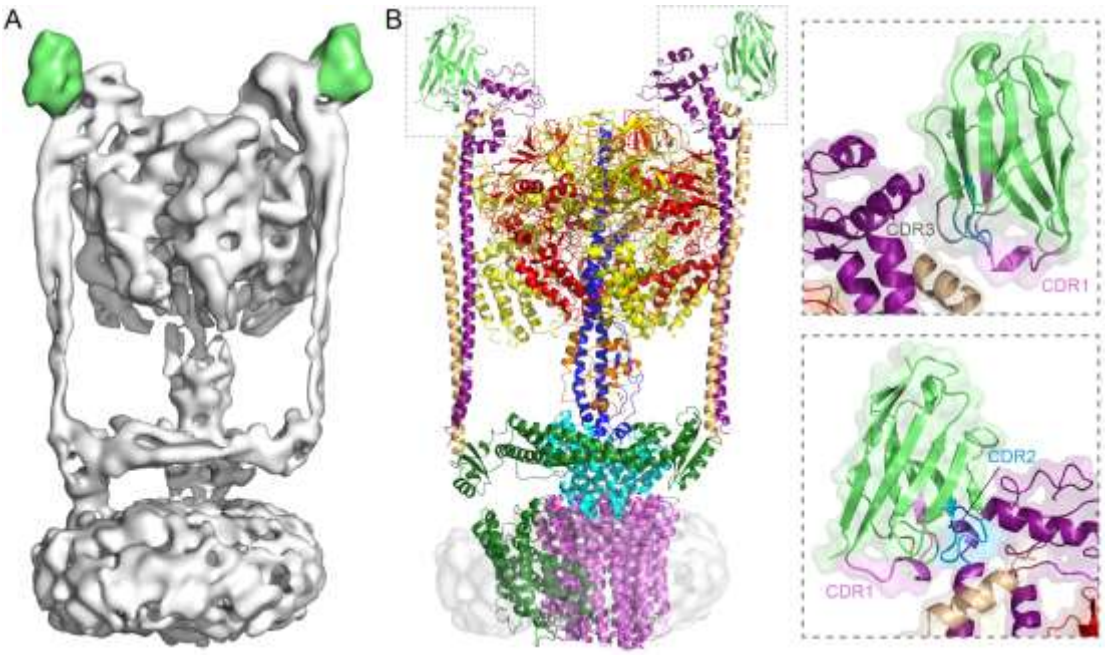

Figure 2: The structure of the *T. thermophilus* A/V-ATPase:dAb complex. (A) Cryo-EM map, with density corresponding to dAbs coloured in lime green. (B) Fitted atomic co-ordinates shown as cartoon with density for the detergent micelle; subunits A in yellow, subunits B in red, subunit C in cyan, subunit D in blue, subunits E in purple, subunit F in orange, subunits G in wheat, subunit I in green, subunits L in magenta, the dAbs in lime green and detergent micelle in grey. Inserts show zoomed view of dAb:ATPase interaction, with CDRs 1, 2 and 3 in pink, cyan and grey respectively.

An atomic model of the *T. thermophilus* A/V-ATPase:dAb complex was made using the deposited structures of *T. thermophilus* A/V-ATPase (pdb code 5gar) (Schep et al., 2016) and the most closely sequence related dAb found in the pdb (pdb code 5hi5) (Liu et al., 2016) modified with swissmodel (Arnold et al., 2006). These models were rigid body docked using Chimera (Pettersen et al., 2004), before truncation of side chains and the C-terminal tail, which was believed to be disordered as in dAb crystal structures (Rouet et al., 2015).

The overall architecture of the complex was very similar to that seen previously (Schep et al., 2016), with the exception that a single dAb can be seen on each of the peripheral stalks (Figure 2). Although the resolution was not sufficient to distinguish the sheets of the immunoglobulin fold, docking into the asymmetric density of the dAb resulted in an orientation that is consistent with all three complementarity-determining regions (CDRs) interacting with the peripheral stalk (Figure 2B).

Fluoroaluminate complexes have been shown to mimic the transition state in several ATP (Ditzel et al., 1998) and GTP (Sondek et al., 1994) hydrolases. The structure of bovine F_1-ATPase inhibited with Mg^{2+}-ADP-AlF_3 has been determined by X-ray crystallography revealing two different states. One showing little difference (Braig et al., 2000) from the native enzyme (Abrahams et al., 1994) and one showing all three catalytic sites occupied by nucleotide along with a large conformational change in the β subunit, believed to represent a catalytic intermediate of the enzyme (Menz et al., 2001). Even though the protein used for cryo-EM structure was produced in the presence of Mg^{2+}, ADP, and AlF_3, its structure showed little difference to that solved in the absence of added nucleotide (Schep et al., 2016). This suggests that the binding

of fluoroaluminate does not appear to require or induce any significant conformational changes of the catalytic domain in A/V-ATPases. However it is possible that the dAb might stabilize and lock the conformation of the complex during purification. Furthermore, due to the limited resolution of the complex, we are unable to say unequivocally that Mg^{2+}-ADP-AlF_3 is present in the active site.

The membrane intrinsic region of the A/V-type ATPase/synthase from *Thermus thermophilus* contains one copy of subunit I and 12 copies of subunit L (Toei et al., 2007). The membrane domain of subunit I has been shown to contain a bundle of helices, arranged in an almost "horizontal" manner (~20-30° to the membrane plane) to facilitate proton transfer (Schep et al., 2016). Although our maps do not show the same level of detail, this ubiquitous protein fold can be observed in slices of the map (Figure 3A) or when segmented to remove the density owing to the detergent micelle and other subunits (Figure 3B).

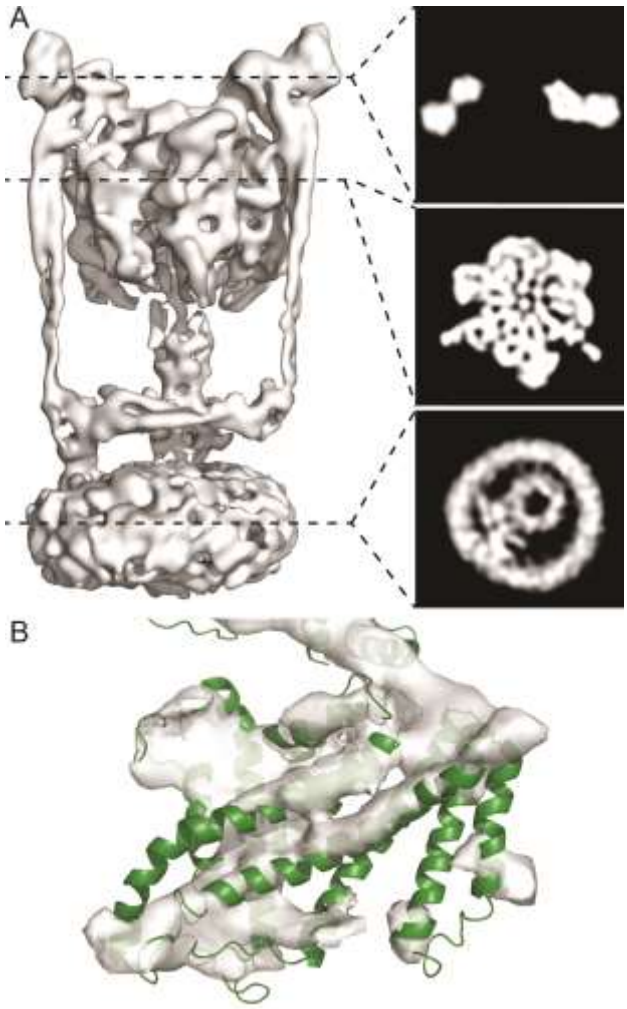

Figure 3: "Slices" and density of the *T. thermophilus* A/V-ATPase:dAb complex. (A) Overall cryo-EM map with slices to highlight data quality and membrane intrinsic subunits. (B) Segmented map to show density (transparent grey) corresponding to the membrane domain of subunit I (green).

Interestingly the density corresponding to the dAbs was some of the strongest in the map with observable density when contoured to only 0.15 e/Å^3, where much of the complex was uninterpretable, with the local resolution (Kucukelbir et al., 2014) being comparable to the soluble domain (Supplementary Figure 3). This suggested very high occupancy for this component, which contrasts with the gas phase using the same sample (Zhou et al., 2014) that showed sub-stoichiometric binding. Although it

is difficult to rule out, no classes were observed during data processing that lacked either one or both dAbs. However, “Class 2” of the first round of 3D classification (Supplementary Figure 2) did appear to contain disassembled complexes, which we were unable to align.

Given the ability of domain antibodies to stabilize and purify a multitude of proteins including G-protein-coupled receptors (Mirzabekov et al., 2000), co-purification followed by cryo-EM analyses would represent an attractive avenue for structure solution, particularly for smaller proteins where the relative increase in overall size due to the addition of antibody is more significant. Furthermore, an increase of asymmetry and homogeneity of the objects could also help data processing. Recent reports describe the utility of dAbs and camelid single domain antibody fragments (termed VHH or nanobodies) in modulating protein quaternary structure (Meyerson et al., 2013) as well as stabilising conformational intermediates of a structurally heterogenous state (Strauss et al., 2016) that were be readily visualised using cryo-EM. Monoclonal fragment antigen-binding (Fab) formats, which contain paired heavy and light chains, have been successfully used in previous cryo-EM studies (Wu et al., 2012). However these Fabs can often be poorly defined due to their intrinsic mobility within the particles (Wu et al., 2012). By contrast dAbs are less flexible due to their single domain architecture bypassing the requirement of a linker region between variable and constant domains. Consequently, single domain antibody modalities may in turn generate better density such as that seen in our reconstruction. Our data also suggests that dAbs could be used with Cryo-Solid Phase Immune Electron Microscopy (Yu et al., 2014), where grids are coated with antibodies for single-step purification and imaging.

In summary, we have determined the cryo-EM structure of a dAb:rotary ATPase complex. This suggests that using dAbs could be a useful strategy for structure determination of other rotary ATPases and perhaps also other protein complexes.

Accession numbers

The atomic coordinates and map were deposited to the pdb and emDB with codes 5TSJ and EMD-8462 respectively.

Acknowledgement

A.G.S was supported by a National Health and Medical Research Council Fellowship APP1090408. D.S. was supported by National Health and Medical Research Council Fellowships APP1004620 and APP1109961. This work was funded by the National Health and Medical Research Council project grants APP1022143 and APP1047004**.** A.W. and S.S. are supported by the Singapore Ministry of Education Academic Research Fund Tier 3 (MOE2012-T3-1-001) and by Nanyang Structural Biology Institute, NTU, Singapore.. M.C. was supported by Australian Research Council Fellowship DE160100608. The Monash Centre for Electron Microscopy is acknowledged for screening of samples.

References:

Abrahams, J.P., Leslie, A.G., Lutter, R., and Walker, J.E. (1994). Structure at 2.8 A resolution of F1-ATPase from bovine heart mitochondria. Nature *370*, 621-628.
Allegretti, M., Klusch, N., Mills, D.J., Vonck, J., Kuhlbrandt, W., and Davies, K.M. (2015). Horizontal membrane-intrinsic alpha-helices in the stator a-subunit of an F-type ATP synthase. Nature *521*, 237-240.
Arnold, K., Bordoli, L., Kopp, J., and Schwede, T. (2006). The SWISS-MODEL workspace: a web-based environment for protein structure homology modelling. Bioinformatics *22*, 195-201.

Bernal, R.A., and Stock, D. (2004). Three-dimensional structure of the intact Thermus thermophilus H+-ATPase/synthase by electron microscopy. Structure *12*, 1789-1798.
Braig, K., Menz, R.I., Montgomery, M.G., Leslie, A.G., and Walker, J.E. (2000). Structure of bovine mitochondrial F(1)-ATPase inhibited by Mg(2+) ADP and aluminium fluoride. Structure *8*, 567-573.
Ditzel, L., Lowe, J., Stock, D., Stetter, K.O., Huber, H., Huber, R., and Steinbacher, S. (1998). Crystal structure of the thermosome, the archaeal chaperonin and homolog of CCT. Cell *93*, 125-138.
Esteban, O., Bernal, R.A., Donohoe, M., Videler, H., Sharon, M., Robinson, C.V., and Stock, D. (2008). Stoichiometry and localization of the stator subunits E and G in Thermus thermophilus H+-ATPase/synthase. J Biol Chem *283*, 2595-2603.
Esteban, O., Christ, D., and Stock, D. (2013). Purification of molecular machines and nanomotors using phage-derived monoclonal antibody fragments. Methods Mol Biol *996*, 203-217.
Hahn, A., Parey, K., Bublitz, M., Mills, D.J., Zickermann, V., Vonck, J., Kuhlbrandt, W., and Meier, T. (2016). Structure of a Complete ATP Synthase Dimer Reveals the Molecular Basis of Inner Mitochondrial Membrane Morphology. Mol Cell *63*, 445-456.
Henderson, R., Sali, A., Baker, M.L., Carragher, B., Devkota, B., Downing, K.H., Egelman, E.H., Feng, Z., Frank, J., Grigorieff, N.*, et al.* (2012). Outcome of the first electron microscopy validation task force meeting. Structure *20*, 205-214.
Kucukelbir, A., Sigworth, F.J., and Tagare, H.D. (2014). Quantifying the local resolution of cryo-EM density maps. Nat Methods *11*, 63-65.
Lau, W.C., and Rubinstein, J.L. (2010). Structure of intact Thermus thermophilus V-ATPase by cryo-EM reveals organization of the membrane-bound V(O) motor. Proc Natl Acad Sci U S A *107*, 1367-1372.
Lau, W.C., and Rubinstein, J.L. (2011). Subnanometre-resolution structure of the intact Thermus thermophilus H+-driven ATP synthase. Nature *481*, 214-218.
Li, X., Mooney, P., Zheng, S., Booth, C.R., Braunfeld, M.B., Gubbens, S., Agard, D.A., and Cheng, Y. (2013). Electron counting and beam-induced motion correction enable near-atomic-resolution single-particle cryo-EM. Nat Methods *10*, 584-590.
Liu, S., Dakin, L.A., Xing, L., Withka, J.M., Sahasrabudhe, P.V., Li, W., Banker, M.E., Balbo, P., Shanker, S., Chrunyk, B.A.*, et al.* (2016). Binding site elucidation and structure guided design of macrocyclic IL-17A antagonists. Sci Rep *6*, 30859.
Mazhab-Jafari, M.T., Rohou, A., Schmidt, C., Bueler, S.A., Benlekbir, S., Robinson, C.V., and Rubinstein, J.L. (2016). Atomic model for the membrane-embedded VO motor of a eukaryotic V-ATPase. Nature *539*, 118-122.
Menz, R.I., Leslie, A.G., and Walker, J.E. (2001). The structure and nucleotide occupancy of bovine mitochondrial F(1)-ATPase are not influenced by crystallisation at high concentrations of nucleotide. FEBS Lett *494*, 11-14.
Meyerson, J.R., Tran, E.E., Kuybeda, O., Chen, W., Dimitrov, D.S., Gorlani, A., Verrips, T., Lifson, J.D., and Subramaniam, S. (2013). Molecular structures of trimeric HIV-1 Env in complex with small antibody derivatives. Proc Natl Acad Sci U S A *110*, 513-518.
Mirzabekov, T., Kontos, H., Farzan, M., Marasco, W., and Sodroski, J. (2000). Paramagnetic proteoliposomes containing a pure, native, and oriented seven-transmembrane segment protein, CCR5. Nat Biotechnol *18*, 649-654.

Nakano, M., Imamura, H., Toei, M., Tamakoshi, M., Yoshida, M., and Yokoyama, K. (2008). ATP hydrolysis and synthesis of a rotary motor V-ATPase from Thermus thermophilus. J Biol Chem *283*, 20789-20796.
Pettersen, E.F., Goddard, T.D., Huang, C.C., Couch, G.S., Greenblatt, D.M., Meng, E.C., and Ferrin, T.E. (2004). UCSF Chimera--a visualization system for exploratory research and analysis. J Comput Chem *25*, 1605-1612.
Rohou, A., and Grigorieff, N. (2015). CTFFIND4: Fast and accurate defocus estimation from electron micrographs. J Struct Biol *192*, 216-221.
Rouet, R., Dudgeon, K., Christie, M., Langley, D., and Christ, D. (2015). Fully Human VH Single Domains That Rival the Stability and Cleft Recognition of Camelid Antibodies. J Biol Chem *290*, 11905-11917.
Schep, D.G., Zhao, J., and Rubinstein, J.L. (2016). Models for the a subunits of the Thermus thermophilus V/A-ATPase and Saccharomyces cerevisiae V-ATPase enzymes by cryo-EM and evolutionary covariance. Proc Natl Acad Sci U S A *113*, 3245-3250.
Scheres, S.H. (2012). RELION: implementation of a Bayesian approach to cryo-EM structure determination. J Struct Biol *180*, 519-530.
Sobti, M., Smits, C., Wong, A.S., Ishmukhametov, R., Stock, D., Sandin, S., and Stewart, A.G. (2016). Cryo-EM structures of the autoinhibited E. coli ATP synthase in three rotational states. Elife *5*.
Sondek, J., Lambright, D.G., Noel, J.P., Hamm, H.E., and Sigler, P.B. (1994). GTPase mechanism of Gproteins from the 1.7-A crystal structure of transducin alpha-GDP-AIF-4. Nature *372*, 276-279.
Stewart, A.G., Laming, E.M., Sobti, M., and Stock, D. (2014). Rotary ATPases--dynamic molecular machines. Curr Opin Struct Biol *25*, 40-48.
Strauss, M., Schotte, L., Karunatilaka, K.S., Filman, D.J., and Hogle, J.M. (2016). CryoEM structures of expanded poliovirus with VHHs sample the conformational repertoire of the expanded state. J Virol.
Toei, M., Gerle, C., Nakano, M., Tani, K., Gyobu, N., Tamakoshi, M., Sone, N., Yoshida, M., Fujiyoshi, Y., Mitsuoka, K*., et al.* (2007). Dodecamer rotor ring defines H+/ATP ratio for ATP synthesis of prokaryotic V-ATPase from Thermus thermophilus. Proc Natl Acad Sci U S A *104*, 20256-20261.
Vinothkumar, K.R., Montgomery, M.G., Liu, S., and Walker, J.E. (2016). Structure of the mitochondrial ATP synthase from Pichia angusta determined by electron cryo-microscopy. Proc Natl Acad Sci U S A.
Wu, S., Avila-Sakar, A., Kim, J., Booth, D.S., Greenberg, C.H., Rossi, A., Liao, M., Li, X., Alian, A., Griner, S.L*., et al.* (2012). Fabs enable single particle cryoEM studies of small proteins. Structure *20*, 582-592.
Yu, G., Vago, F., Zhang, D., Snyder, J.E., Yan, R., Zhang, C., Benjamin, C., Jiang, X., Kuhn, R.J., Serwer, P*., et al.* (2014). Single-step antibody-based affinity cryo-electron microscopy for imaging and structural analysis of macromolecular assemblies. J Struct Biol *187*, 1-9.
Zhao, J., Benlekbir, S., and Rubinstein, J.L. (2015). Electron cryomicroscopy observation of rotational states in a eukaryotic V-ATPase. Nature *521*, 241-245.
Zhou, M., Politis, A., Davies, R.B., Liko, I., Wu, K.J., Stewart, A.G., Stock, D., and Robinson, C.V. (2014). Ion mobility-mass spectrometry of a rotary ATPase reveals ATP-induced reduction in conformational flexibility. Nat Chem *6*, 208-215.

Supplementary Figures

Cryo-EM analysis of a domain antibody bound rotary ATPase complex
Davies et al.

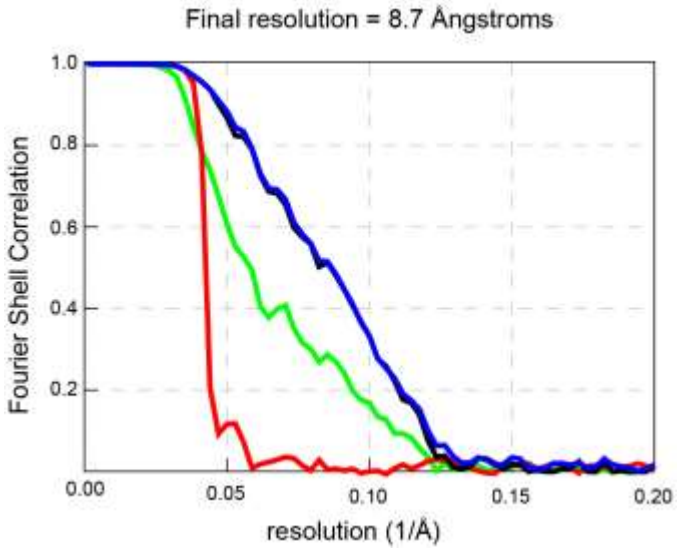

Supplementary Figure 1: FSC curves showing the effects of masking on the refined map, with the gold-standard, corrected FSC curve (black), FSC of the unmasked map (green), FSC of the masked map (blue), and FSC of the phase-randomized masked map (red).

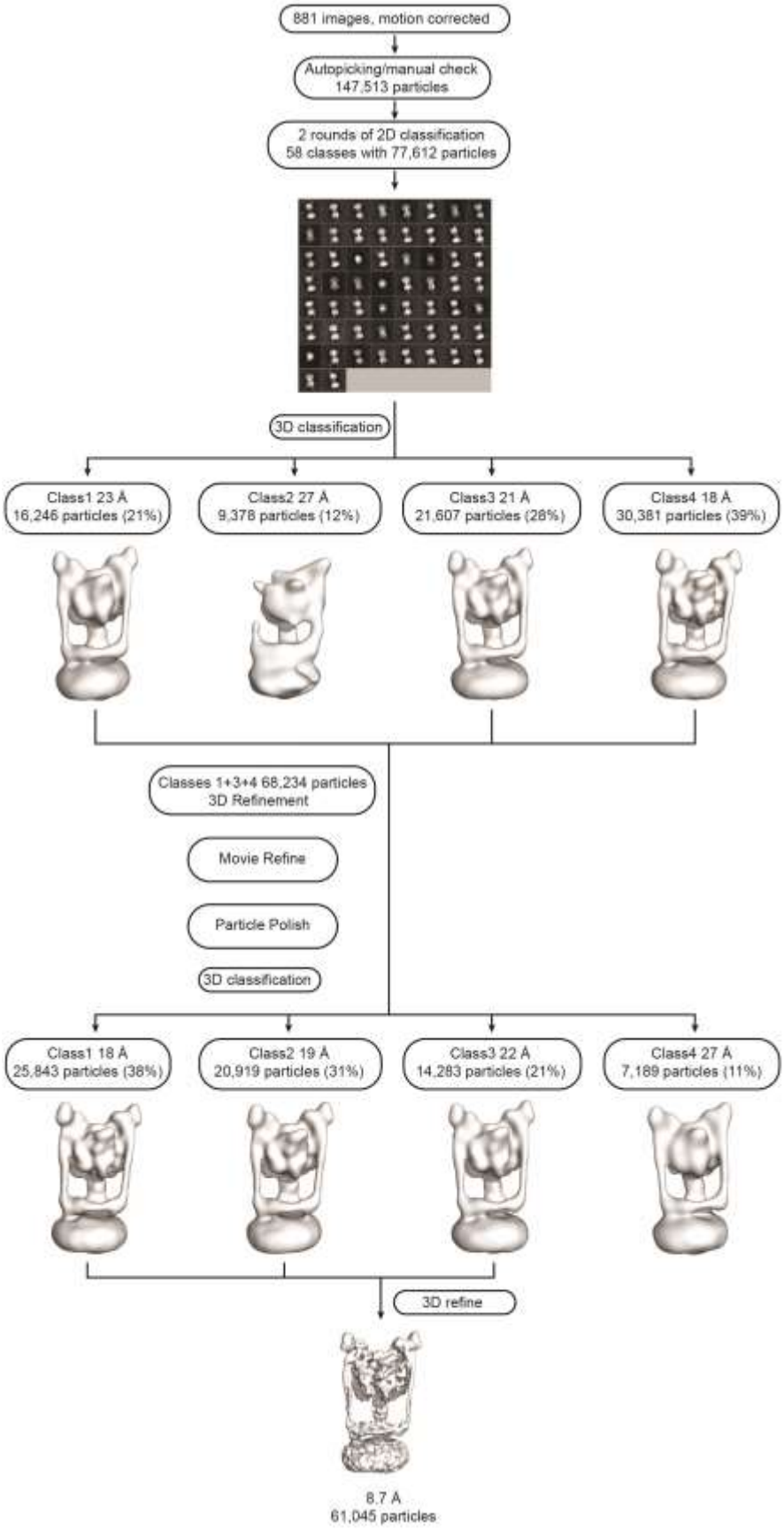

Supplementary Figure 2: Flowchart summarizing data analysis

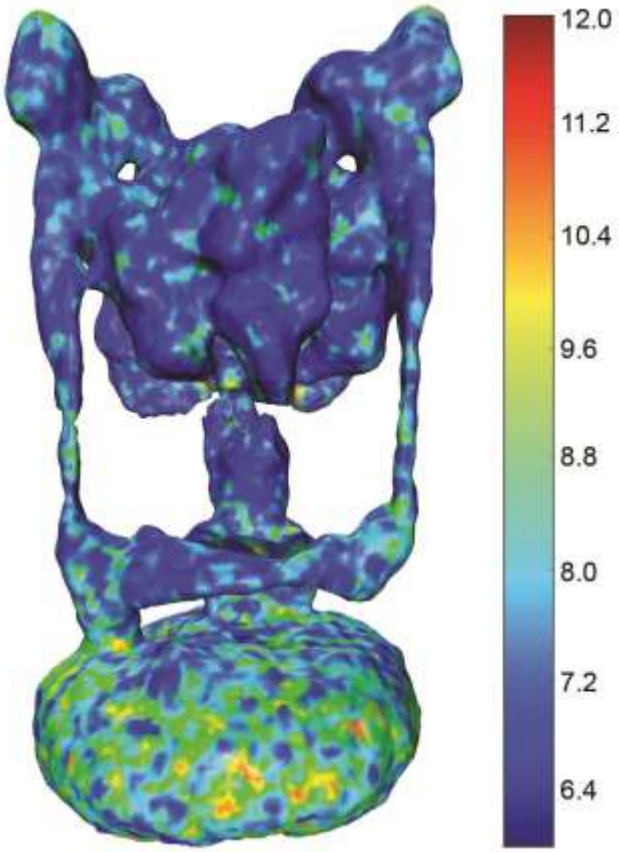

Supplementary Figure 3: Local resolution plot with scale made using ResMap (Kucukelbir et al., 2014).

Kucukelbir, A., Sigworth, F.J., and Tagare, H.D. (2014). Quantifying the local resolution of cryo-EM density maps. Nat Methods *11*, 63-65.